RMetS
Royal Meteorological Society

Summertime precipitation over northern Australia in AMIP simulations from CMIP5

D. Ackerley,[a,b]* G. Berry,[b] C. Jakob,[a,b] M. J. Reeder[a,b] and J. Schwendike[b]
[a]*ARC Centre of Excellence for Climate System Science, Monash University, Clayton, Victoria, Australia*
[b]*School of Earth, Atmosphere and Environment, Monash University, Clayton, Victoria, Australia*

*Correspondence to: D. Ackerley, School of Earth, Atmosphere and Environment, Monash University, Wellington Road, Clayton, Victoria 3800, Australia. E-mail: duncan.ackerley@monash.edu

Tropical precipitation is caused by many processes that occur over a wide range of temporal and spatial scales. Such processes vary from local, diurnal convection driven by a destabilisation of the boundary layer to planetary-scale systems that result in rainfall over many days. It is therefore important to assess whether general circulation models (GCMs) can represent these processes given that such models are routinely used to project future rainfall in the low latitudes. In this study, we evaluate the rainfall and circulation characteristics of ten GCMs from the Coupled Model Intercomparison Project Phase 5 (CMIP5) over northern Australia. This work shows that the diurnal cycle of the low-level (925 hPa) flow around the heat low is represented well by the models but the timing of precipitation is not (triggered too early). There is also evidence that mid-level synoptic systems that are responsible for *initiating* rain in the observations are also present in all of the models. Nevertheless, the biases in the modelled seasonal mean precipitation seem to be linked to the strength of both the meridional flow into northern Australia and the vertical mass flux. Furthermore, there is also evidence that the representation of convection in these models is likely contributing to both the precipitation and circulation errors over northern Australia.

Key Words: rainfall; circulation; CMIP5; north Australia; diurnal cycle; AMIP
Received 20 June 2014; Revised 24 September 2014; Accepted 29 September 2014; Published online in Wiley Online Library 13 December 2014

1. Introduction

In northern Australia (north of 30°S in this study), the majority of the annual rain falls in the austral summer (December, January and February; DJF) monsoon (Suppiah, 1992). The rainfall can be caused by many processes such as: convection triggered by solar heating and a destabilisation of the boundary layer (Keenan and Carbone, 2008); convection forced by convergence into the nocturnal heat low circulation (Berry *et al.*, 2011); the vertical motion and destabilisation of the atmosphere by synoptic and large-scale tropical systems such as the Madden–Julian Oscillation (MJO; Wheeler *et al.*, 2009); and also the intrusion of extratropical disturbances into the Tropics and Subtropics (Berry *et al.*, 2012). A proper representation of Australian summertime rainfall in general circulation models (GCMs) requires that they accurately simulate the conditions that force rainfall over the continent.

Previous modelling work by Ackerley *et al.* (2014) evaluated the diurnal cycle, moisture transports and large-scale circulation patterns over northern Australia in the Australian Community Climate and Earth System Simulator version 1.3 (ACCESS1.3) GCM, in order to determine whether the model accurately represented the physical mechanisms that lead to rainfall in this region of the globe. In an approach similar to Ackerley *et al.* (2014), the diurnal cycle, convection, moisture transports and low-to-mid-level circulation features that are responsible for rainfall over northern Australia are evaluated in a selection of GCM simulations from the Coupled Model Intercomparison Project Phase 5 (CMIP5; Taylor *et al.*, 2012).

The aims of this work are threefold. The first aim is to assess whether the models can represent the climatological mean, frequency, daily accumulation and the diurnal cycle of rain over northern Australia. The second aim is to ascertain if the models properly represent the seasonal and diurnal circulation characteristics over the Australian continent. The third aim is to identify whether the moisture sources and synoptic systems responsible for initiating rain are represented well.

The models used in this study are given in section 2. Descriptions of the precipitation, circulation, moisture transports and the synoptic systems responsible for initiating rain are given in sections 3–5. A discussion of the results in sections 3–5 is given in section 6 and the conclusions are given in section 7.

2. Models and data

2.1. Models

The models used in this study, their horizontal and vertical resolutions, and their relevant references are listed in Table 1. Ten different model simulations were chosen as they have 3 hourly rainfall and 6 hourly circulation diagnostics available on all model levels. All of the model simulations are run with Atmospheric Model Intercomparison Project (AMIP) boundary conditions

Table 1. The models used, horizontal and vertical resolution, relevant references and labels for subsequent figures.

Model	Resolution		References	Model label
	Horizontal	No. of levels		
ACCESS1.0	N96, 1.875° × 1.25°	38	Martin *et al.* (2011) and Bi *et al.* (2013)	A
ACCESS1.3	N96, 1.875° × 1.25°	38	Hewitt *et al.* (2011) and Bi *et al.* (2013); Kowalczyk *et al.* (2013)	B
BCC-CSM1-1	T42, 2.81°	26	Wu *et al.* (2010) and Xin *et al.* (2013)	C
BCC-CSM1-1-m	T160, 1.0°	26	Wu *et al.* (2010) and Xin *et al.* (2013)	D
BNU-ESM	T42, 2.81°	26	Ji *et al.* (2014)	E
CCSM4	1.25° × 0.9°	26	Gent *et al.* (2011)	F
IPSL-CM5A-LR	3.75° × 1.875°	39	Dufresne *et al.* (2013)	G
MIROC5	T85, 1.4°	40	Watanabe *et al.* (2010)	H
MRI-CGCM3	T159, 1.125°	48	Yukimoto *et al.* (2012)	I
NorESM1-M	2.5° × 1.9°	26	Bentsen *et al.* (2013)	J

with prescribed sea-surface temperatures (SSTs) and sea ice from 1978 to 2008 (Gates, 1992; Gates *et al.*, 1999; Taylor *et al.*, 2000). The AMIP simulations are used here in order to minimise errors in the large-scale circulation that may arise from biases in the SST field produced by the fully dynamical ocean models (e.g. the cold-tongue bias in the tropical Pacific; Irving *et al.*, 2011; Grose *et al.*, 2014).

Although all simulations are independent, some of the models (Table 1) share common parametrization schemes, which may result in similar modelled climates. For example, the ACCESS1.0 simulation uses the HadGEM2(r1.1) physics (Martin *et al.*, 2011) whereas ACCESS1.3 uses both a different land-surface scheme (Community Atmosphere Biosphere Land Exchange version 1.8, CABLE; Kowalczyk *et al.*, 2006, 2013) and a cloud scheme known as the 'prognostic cloud fraction and prognostic condensate' scheme (PC2; Wilson *et al.*, 2008a). Moreover, the BCC-CSM1-1, BCC-CSM1-1-m, BNU-ESM, CCSM4 and NorESM1-M models use different versions of the Community Atmospheric Model (CAM) physics. For example, The BCC-CSM1-1 and BCC-CSM1-1-m simulations (the former is a lower-resolution version of the latter) were developed from version 3 of CAM and BNU-ESM from version 3.5. Both CCSM4 and NorESM1-M use version 4 of CAM; however, the aerosol scheme used in NorESM1-M is different from the one used in CCSM4. The remaining models, IPSL-CM5A-LR, MIROC5 and MRI-CGCM3, have all been developed independently of each other and the groups of models highlighted above.

Finally, all model data are re-gridded to a common 2.5° × 2.5° grid (for comparison against each other and the observational datasets described below) and only data from DJF for the years 1979/1980–2007/2008 are used.

2.2. Observations and reanalyses

The zonal and meridional flow and geopotential heights (at the various levels described in the text) from the European Centre for Medium-Range Weather Forecasts Interim Reanalysis (ECMWF ERA-Interim; Dee *et al.*, 2011) are used to evaluate the model simulations described in section 2.1. The reanalysis data for each DJF from 1979/1980 to 2007/2008 are re-gridded from the original 1.5° × 1.5° to the common 2.5° × 2.5° applied to the models (section 2.1).

Precipitation climatologies for the Australasian region are calculated from the Climate Prediction Centre Merged Analysis of Precipitation (CPC CMAP; Xie and Arkin, 1997), which is derived from a combination of rain-gauge and satellite-based instruments. Monthly mean data at 2.5° × 2.5° resolution for each DJF from 1979/1980 to 2007/2008 are used.

In order to assess the diurnal cycle of rainfall over the Australian continent, 6 hourly rainfall rates from the CPC morphing method dataset (CMORPH; Joyce *et al.*, 2004) are used for the period 1998–2012. The CMORPH data have a spatial resolution of 0.25° × 0.25° between ±60° latitude, which are also re-gridded to the common 2.5° × 2.5° grid used in the evaluation of the ERA-Interim reanalysis and the models. The maximum in the satellite-derived precipitation from CMORPH is known to be delayed slightly relative to surface observations (Dai *et al.*, 2007); however, it has been shown in Ackerley *et al.* (2014) that the peak in 3 hourly CMORPH rainfall data agrees well with surface-based gauges over Australia, and therefore the 6 hourly estimates are unlikely to suffer from the problem highlighted in Dai *et al.* (2007). Composites of CMOPRH precipitation on wet days are used to assess the frequency and accumulation of daily rain, and the diurnal cycle of precipitation. Days on which the rainfall is less than 0.2 mm are not considered as rain days by the Australian Bureau of Meteorology (BoM) and are defined to be dry days in this study. Conversely, a day is considered to be wet if the rainfall is greater than or equal to 0.2 mm.

Finally, daily data from the Australian Water Availability Project (AWAP; Jones *et al.*, 2009) from 1979/1980 to 2007/2008 are used to identify the synoptic conditions responsible for initiating rain over the Australian continent. As with the other model, reanalysis and observational fields, the AWAP data are re-gridded from their original 0.05° × 0.05° resolution to 2.5° × 2.5°. The definition of a wet day is modified for the composites of ERA-Interim geopotential height and circulation fields using AWAP data. A day is considered to be the initial wet day (init) if the rainfall is greater than or equal to 0.2 mm but, if there are subsequent wet days, only this first day is used to produce the circulation composites. This is done to isolate and identify the conditions necessary to *initiate* a precipitation event from the atmospheric response to that precipitation. The same method of separating init and dry days is also applied to each of the models to produce corresponding rainfall and circulation composites.

All references to local time for the diurnal cycle of precipitation and circulation are given in Australian Western Standard Time (AWST), which is 8 h ahead of the Coordinated Universal Time (UTC+8).

3. Precipitation

3.1. Climatology

Although northern Australia is the focus of this study, the average rainfall for DJF (1979/1980–2007/2008) from CMAP over the entire Australian land surface and surrounding ocean is plotted in Figure 1(a) as it places the following analysis in a broader context. The climatological precipitation over Australia is higher in the north than the south, and the east coast is also wetter than the west coast southward of approximately 20°S. All of the models have higher DJF-mean precipitation over the north and east of the Australian continent than over the south and west. Moreover, the pattern correlations between each model and CMAP (for Australian-wide precipitation) are all greater than 0.89.

The differences (mm day^{-1}) between each model-simulated rainfall and CMAP are plotted in Figure 1(b–k). Five models

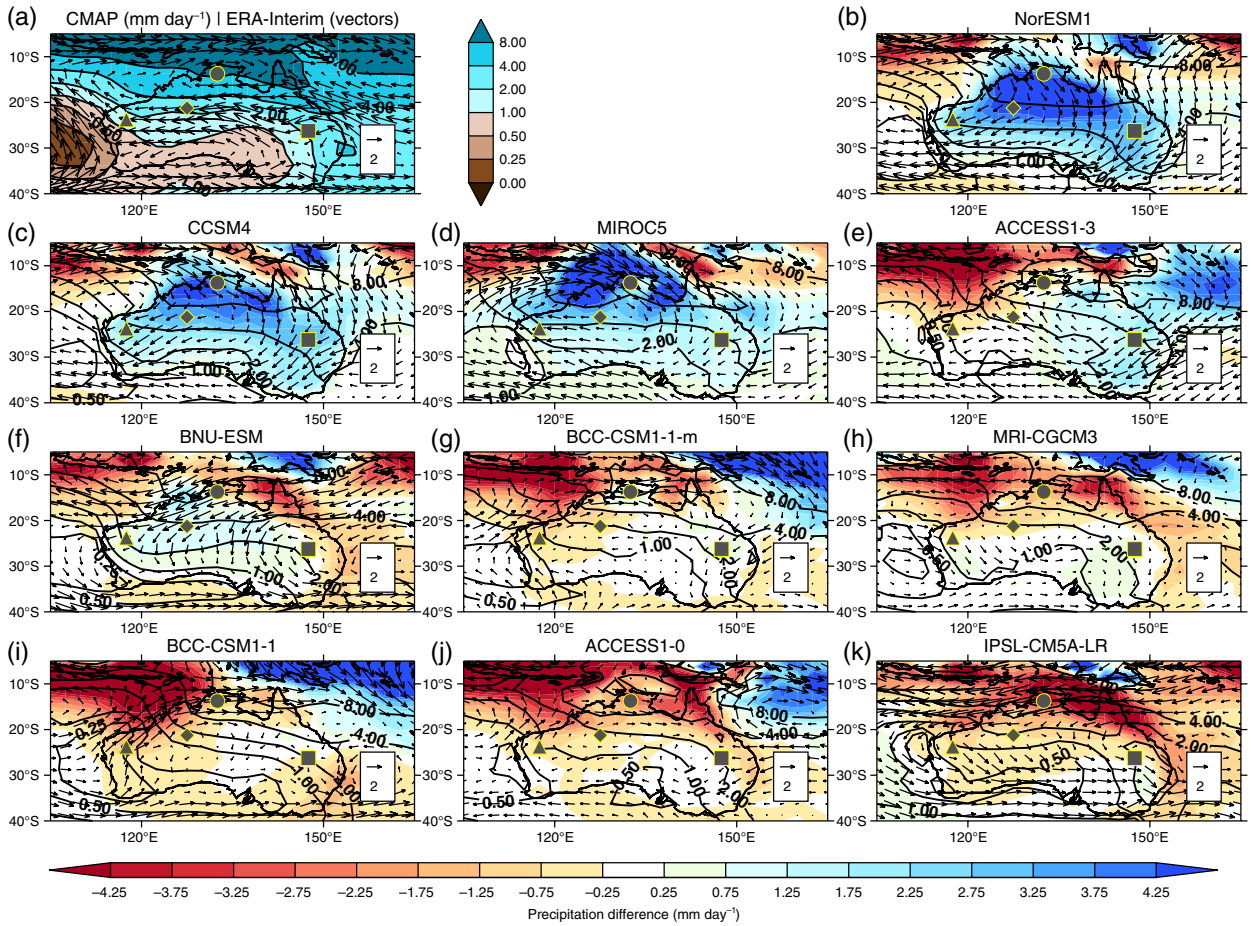

Figure 1. (a) The DJF-mean precipitation (mm day^{-1}, colour shading) and 850 hPa wind field (m s^{-1}, arrows) from CMAP and ERA-Interim, respectively (1979/1980–2007/2008). (b)–(k) The absolute (mm day^{-1}, solid contours) and difference in precipitation relative to CMAP (mm day^{-1}, colour shading), and the difference in the 850 hPa wind field (m s^{-1}, arrows) relative to ERA-Interim for each of the models given in Table 1. The symbols denote the following points described in section 6: Eastern Point (EP) –□, Western Point (WP) –△, Top End (TE) –○ and Nocturnal Peak (NP) –◇.

(NorESM1-M, CCSM4, MIROC5, ACCESS1.3 and BNU-ESM; Figure 1(b–f)) are too wet over most of the land surface. Moreover, the rainfall biases relative to CMAP are greater than 50% to the north of 30°S in NorESM1-M, CCSM4 and MIROC5. The other five models have dry biases across the north (BCC-CSM1-1-m, MRI-CGCM3, BCC-CSM1-1, ACCESS1.0 and IPSL-CM5A-LR; Figure 1(g–k)). The dry bias extends over much of the land surface north of 30°S in ACCESS1.0 and IPSL-CM5A-LR and to the north of 20°S in MRI-CGCM3 where these models are approximately 10–30% drier than CMAP. The spatial patterns of positive and negative biases in Figure 1(b–k) are also visible when the modelled precipitation is compared against two other precipitation datasets (the Global Precipitation Climatology Project and AWAP, not shown). This implies that the differences in Figure 1(b–k) are primarily the result of deficiencies in the models and not the observational errors.

The mean precipitation northward of 30°S is given in Table 2 for CMAP and each model. The NorESM1-M, CCSM4 and MIROC5 models are more than 2 mm day^{-1} wetter than the CMAP estimate whereas ACCESS1.0, BCC-CSM1-1 and IPSL-CM5A-LR are at least 0.6 mm day^{-1} drier. The root-mean-squared errors (RMSEs) for each model relative to CMAP, northward of 30°S over Australia, are also listed in Table 2. BCC-CSM1-1-m has the lowest RMSE (0.51 mm day^{-1}), which is due to the low precipitation biases over much of the land surface (Figure 1(g)). The MRI-CGCM3 (0.81 mm day^{-1}) and ACCESS1.3 (0.87mm day^{-1}) models have the second and third lowest RMSE. The NorESM1-M, CCSM4 and MIROC5 models have the three highest values of RMSE (3.07, 2.47 and 2.38 mm day^{-1}, respectively), which is associated with too much precipitation over most of the Australian continent north of 30°S (Figure 1(b–d)). The IPSL-CM5A-LR model has the fourth highest RMSE, which is primarily associated with the dry bias to the north of 30°S (Figure 1(k)).

The errors in the precipitation (Table 2) do not appear to be resolution dependent (Table 1). For example, the BCC-CSM1-1-m, CCSM4, MIROC5 and MRI-CGCM3 models have the highest horizontal resolution but have the first, ninth, eighth and second lowest RMSE values, respectively. Conversely, the ACCESS1.0 model has a resolution equal to that of ACCESS1.3, but has the sixth lowest RMSE for Australian precipitation whereas ACCESS1.3 has the third lowest.

3.2. *Rain-day frequency and daily accumulation*

Studies by Sun *et al.* (2006) and Stephens *et al.* (2010) have both shown that GCMs and weather prediction models produce rain too frequently while underestimating its daily accumulation. Frequent, low-intensity rainfall in the models has been attributed to the premature triggering of moist convection as the boundary layer is heated during the day (Dai and Trenberth, 2004; Dai, 2006). The frequency and accumulated daily precipitation in the models are therefore assessed in this section.

The total frequency (%) of rainfall days greater than 0.2 mm from CMORPH is plotted in Figure 2(a). Equatorward of 20°S, rainfall occurs on 45% of the days and over the far north of the continent (north of 15°S) it occurs on more than 60% of the days. The models reproduce this pattern of increasing rainfall frequency from the south of the continent to the north; however, the rainfall frequency is typically too high in the models over the land surface, particularly in the NorESM1-M, CCSM4, MIROC5, BNU-ESM and IPSL-CM5A-LR models where precipitation occurs on more than 90% of the simulated DJF days (Figure 2(b–d,f,k)). Overlaid in Figure 2 is the frequency of days (%) where convective rainfall is also greater than 0.2 mm, which matches the distribution of the total rainfall frequencies. This

Table 2. DJF-mean precipitation (P) and root-mean-squared-error (RMSE) values for precipitation over the northern half of Australia (from 30°S northward) for each model relative to CMAP. $V_{13.75S}$ is the mean northward air flow at 850 hPa between 120 and 150°E. The last four columns contain the DJF-mean precipitation at the Eastern Point (EP), Western Point (WP), Top End (TE) and Nocturnal Peak (NP) grid points for CMAP and each of the models (referred to in section 6).

Model	P	RMSE	$V_{13.75S}$	EP	WP	TE	NP
CMAP	3.08	–	0.28[a]	2.27	1.73	8.86	2.33
NorESM1-M	6.41	3.07	−1.16	5.22	4.59	12.40	7.01
CCSM4	5.78	2.47	−0.95	5.06	3.69	12.84	5.80
MIROC5	5.31	2.38	−0.59	3.83	3.46	10.79	4.76
ACCESS1.3	3.58	0.87	0.66	3.58	1.44	8.69	2.42
BNU-ESM	3.39	0.95	−0.36	2.22	2.30	8.00	3.56
BCC-CSM1-1-m	2.89	0.51	0.40	2.58	0.89	9.72	1.96
MRI-CGCM3	2.65	0.81	0.57	2.86	1.30	7.24	1.80
BCC-CSM1-1	2.41	0.89	0.79	2.05	0.31	7.51	1.53
ACCESS1.0	2.14	1.20	0.81	2.10	1.07	6.13	1.65
IPSL-CM5A-LR	1.79	1.67	−0.04	1.92	0.97	4.87	1.86

[a] From ERA-Interim. Units for $V_{13.75S}$ are m s^{-1}; all others are mm day^{-1}.

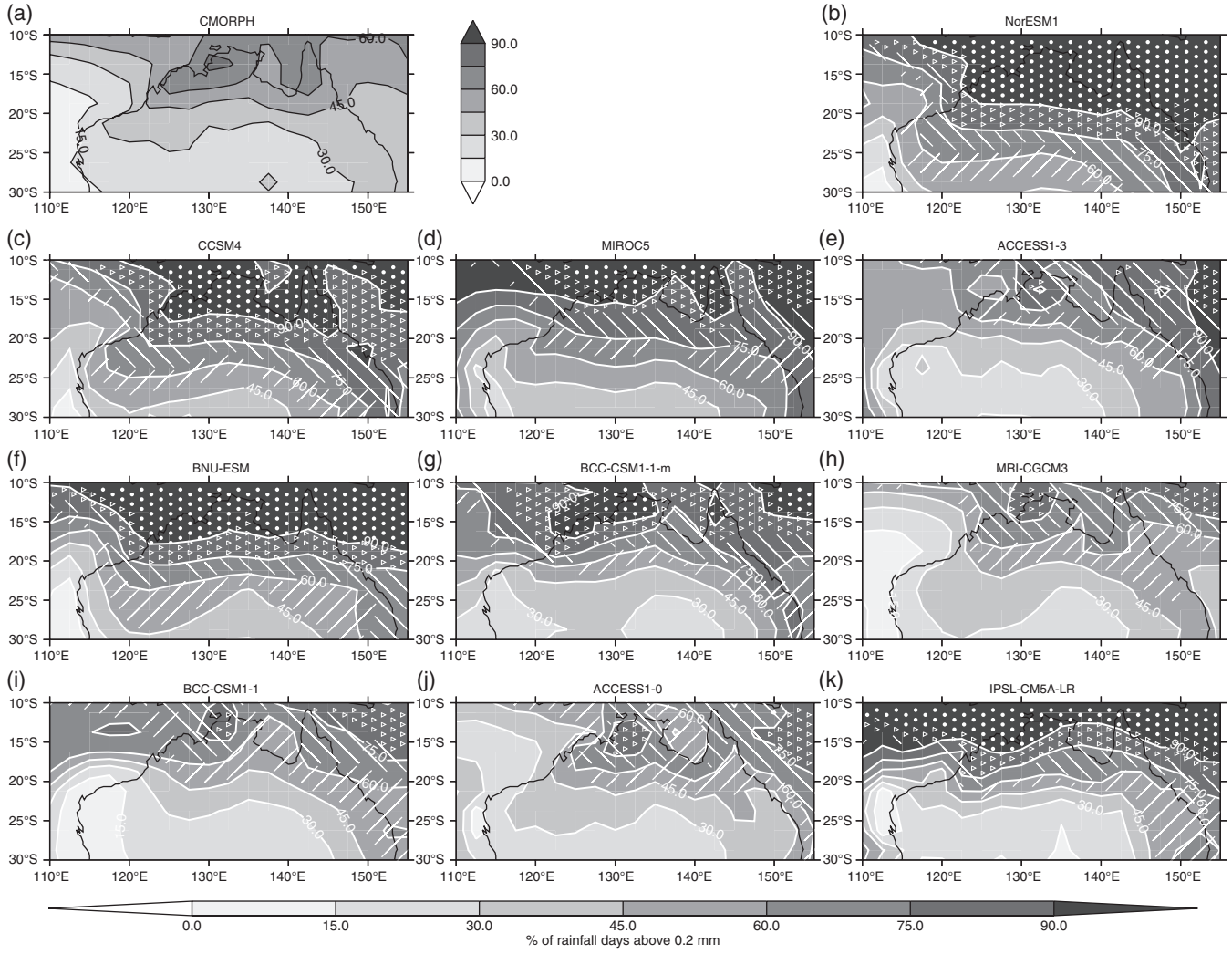

Figure 2. The total frequency of occurrence of wet days for DJF for (a) CMORPH (1998–2012) and (b)–(k) for each of the models (1979–2008). The contour interval is 15%. Overlaid are the corresponding frequencies of occurrence for convective rainfall ≥0.2 mm day^{-1} where //= 45–60%, \\= 60–75%, ▷= 75–90% and ● =>90%.

suggests that it may be the frequent activation of convection in these models that causes the rainfall to occur too often.

The mean daily rainfall in CMOPRH (mm day^{-1}) is given in Figure 3(a) and the differences between each model and CMORPH are shown in Figure 3(b–k). In all models, the daily rainfall is too low over northern Australia, especially in IPSL-CM5A-LR where the frequency is too high (Figure 2(k)). The NorESM1-M, CCSM4 and MIROC5 models all have the highest daily rainfall, relative to the other models, and IPSL-CM5A-LR and ACCESS1.0 have the lowest daily rainfall over northern Australia.

3.3. *Diurnal cycle*

Composites of 6 h percentage contribution of rainfall between 0500 and 1100, 1100 and 1700, 1700 and 2300, and 2300 and 0500 AWST to the total daily accumulation from CMORPH are plotted in Figure 4 (dry days are not included in these composites). This relative contribution is used in order to highlight the timing of precipitation in the observations and the models, regardless of the actual total amounts. The rainfall is calculated between ±3 h of the reanalysis output (at 0800, 1400, 2000 and 0200 AWST) so that any local circulation features responsible for the rain can

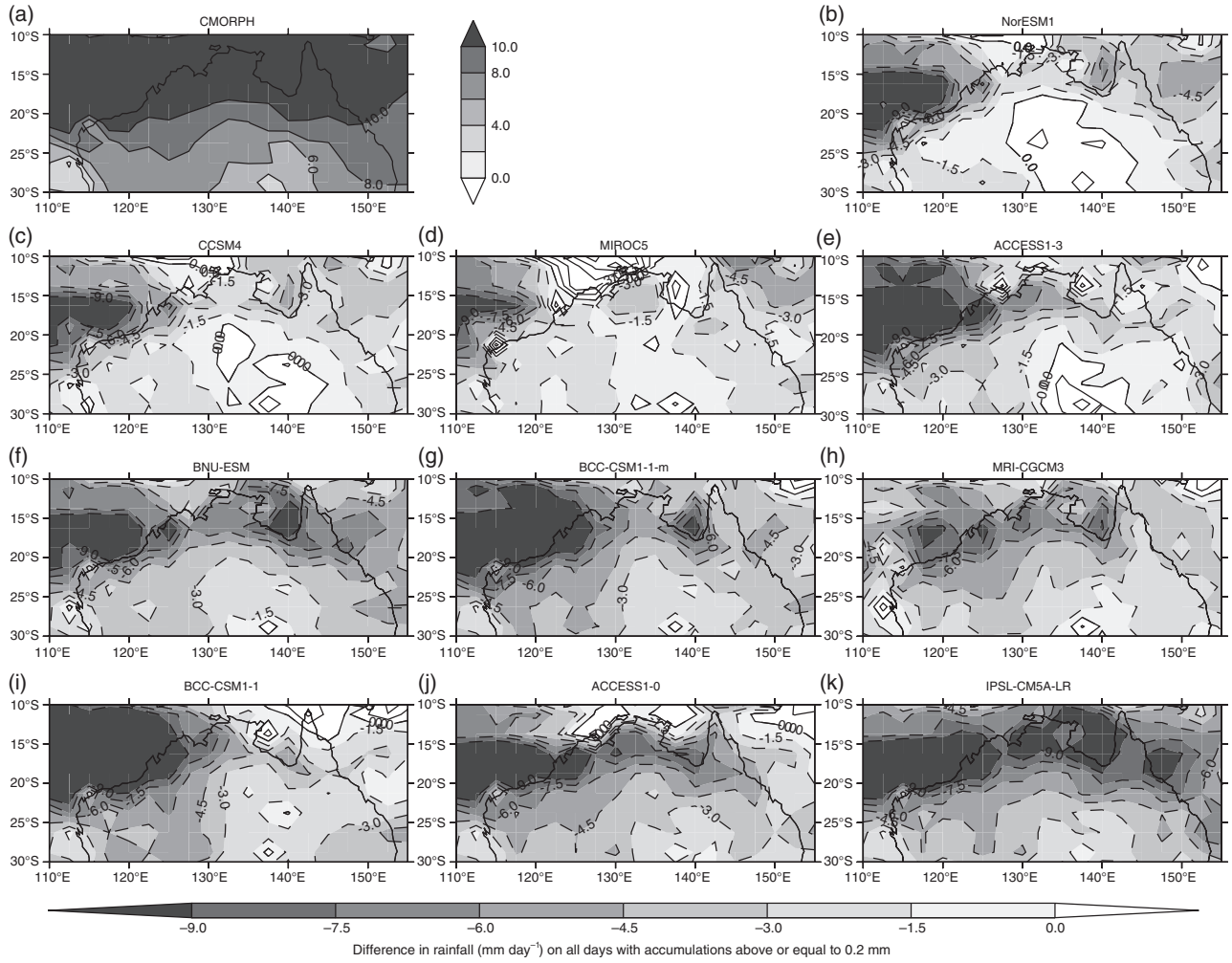

Figure 3. The difference between the DJF-mean daily rainfall (mm day^{-1}) on wet and dry days over all available years for (a) CMORPH (1998–2012) and (b)–(k) for each of the models (1979–2008). Negative (positive) values have dashed (solid) contours, with interval 1.5 mm day^{-1}.

be identified (section 4.3). Furthermore, grid points where more than 25% of the daily accumulated convective rainfall occurs in each 6 h period are stippled in Figure 4 to identify whether the rainfall is caused by convection in the models.

Less than 20% of the CMORPH-derived climatological daily rain falls between 0500 and 1100 AWST over much of northern Australia (Figure 4, first column), which is unsurprising given that at this time it is unlikely that the surface has been heated enough to destabilise the boundary layer and initiate convection. The models (on average) already produce more than 25% of their daily rainfall between 0500 and 1100 AWST over parts of eastern Australia (Figure 4, first column). The rain is likely to be convective (as shown by the stippling in Figure 4) and this premature triggering of convection, relative to observations, is a common problem in GCMs (Yang and Slingo, 2001; Dai and Trenberth, 2004; Dai, 2006; Brown *et al.*, 2010; Stratton and Stirling, 2012).

By 1100–1700 AWST more than 25% of the mean rainfall occurs to the east of 130°E over Australia in CMORPH (Figure 4, second column) and less than 25% to the west. All of the models have more than 25% of the grid-point rainfall occurring across most of the continent between 1100 and 1700 AWST, except in ACCESS1.0 where it is largely confined to the north and east. Nonetheless, the stippling indicates that all models have widespread convective activity between these times.

Between 1700 and 2300 AWST, more than 25% of the mean daily rain falls over most of the continent to the north of 30°S in CMORPH (Figure 4, third column). The precipitation maximum between 1700 and 2300 AWST is centred at approximately 115°E, 22.5°S. Similarly, all but one of the models (IPSL-CM5A-LR) have a region of higher mean precipitation (more than 20% of the daily accumulation) to the west of 130°E and between 20 and 25°S. The stippling indicates that there is still some convective activity at this time, although there is little rainfall or convective activity in the IPSL-CM5A-LR simulation between 1700 and 2300 AWST as the majority of the precipitation falls between 0500 and 1700 AWST.

From 2300 to 0500 AWST rainfall fractions are greater than 25% between 120 and 150°E in CMORPH (Figure 4, fourth column). Both ACCESS1.0 and ACCESS1.3 have high rainfall fractions in the western half of the continent between 2300 and 0500 AWST. Similarly, more than 25% of the daily rainfall occurs over the continent in MRI-CGCM3 between 2300 and 0500 AWST. The rainfall fractions (2300–0500 AWST) in the remaining models (BCC-CSM1-1, BCC-CSM1-1-m, BNU-ESM, CCSM4, MIROC5 and NorESM1-M) between 120 and 150°E are too low relative to CMORPH. Nonetheless, the precipitation fractions along the northern and eastern coasts in both the BCC-CSM1-1 and BCC-CSM1-1-m simulations are much higher than those in CMORPH, which suggests these models may have problems representing rainfall adjacent to the coast.

4. Horizontal and vertical circulation features

The rainfall features identified above over northern Australia during DJF are affected by the local heat low circulation and its internal dynamics, the larger-scale monsoon circulation (horizontal and vertical), the availability and transport of moisture onto the continent, and the development of synoptic systems that initiate rainfall. Each of these factors are discussed in this and the following sections.

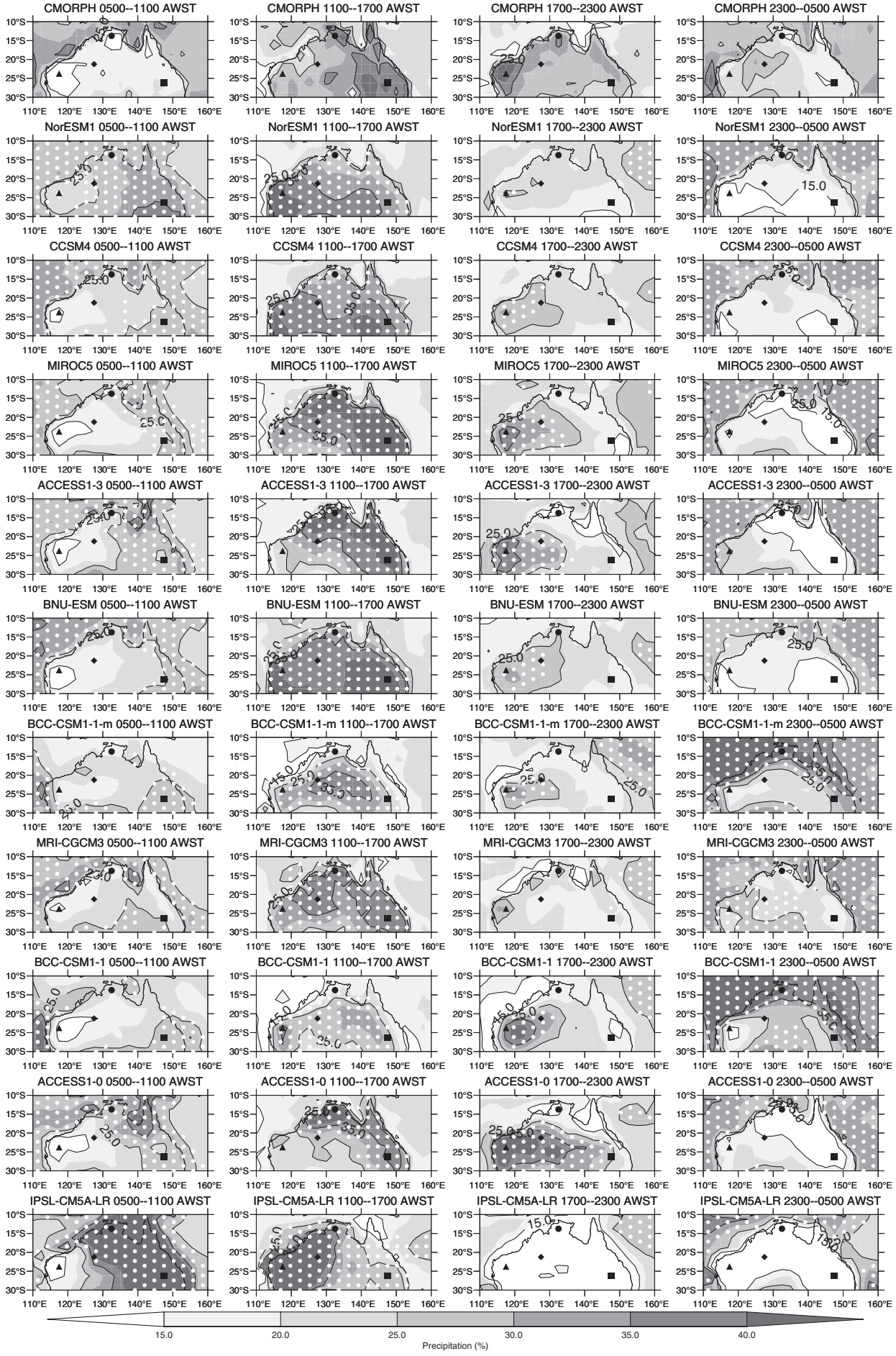

Figure 4. The mean relative contribution of 6 hourly precipitation accumulations to the daily rainfall (%, dry days are excluded) from CMORPH and from each of the models for time intervals (column 1) 0500–1100 AWST, (column 2) 1100–1700 AWST, (column 3) 1700–2300 AWST and (column 4) 2300–0500 AWST. Stippling on the figures for the models denotes grid points where the 6 hourly convective precipitation $\geq$ 25% of the total convective precipitation. The symbols denote the following points described in section 6: Eastern Point (EP) –□, Western Point (WP) –△, Top End (TE) –○ and Nocturnal Peak (NP) –◇.

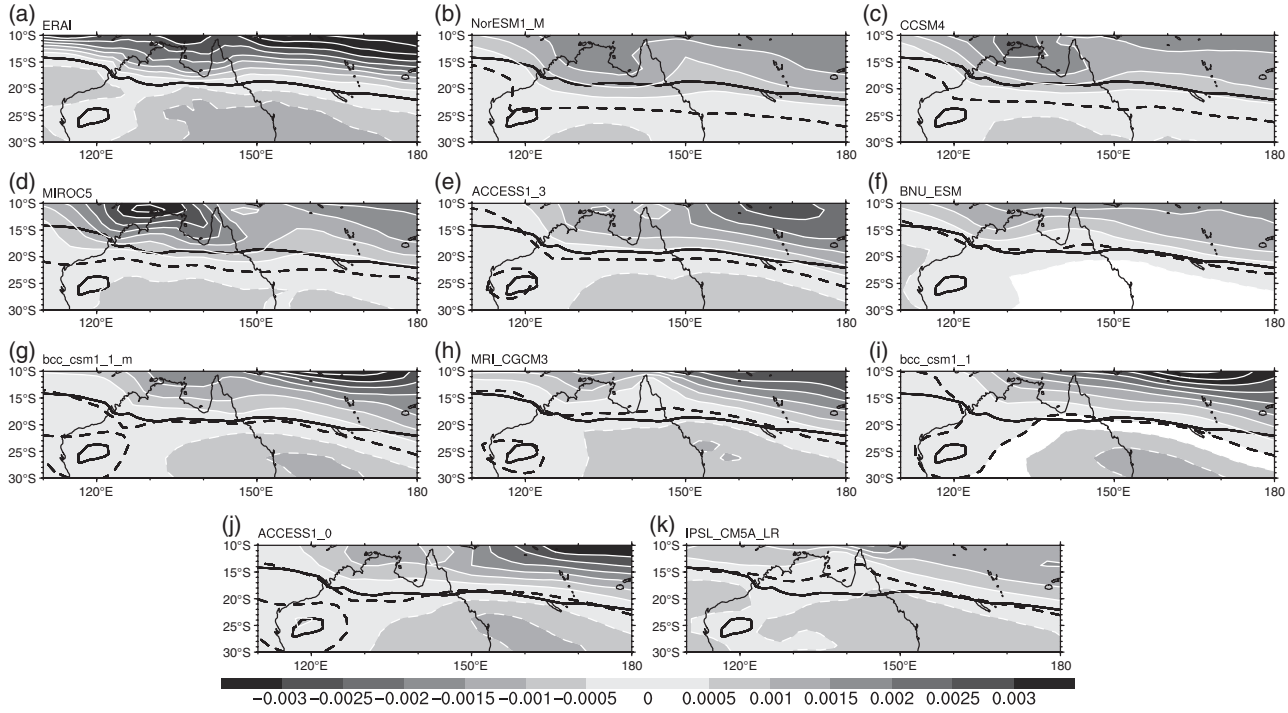

Figure 5. The ψ-Hadley circulation derived using the method in Schwendike *et al.* (2014). The meridional mass flux (kg m^{-2} s^{-1}) at 500 hPa for the season DJF (1979–2008) calculated from (a) the ERA-Interim reanalysis and (b)–(k) from the CMIP5 models. The bold black line in all plots indicates the zero line in the ERA-Interim dataset and the dashed line is the zero line in the respective CMIP5 simulations. Positive (negative) mass fluxes are denoted by solid (dashed) white contours (contour separation is defined in the shade key).

4.1. *Climatological circulation at 850 hPa*

The climatological flow at 850 hPa is plotted in Figure 1(a). The monsoon cyclone is centred at approximately 13°S, 130°E (as has also been identified in Klingaman *et al.*, 2012) with easterly flow over the Australian continent to the south and westerlies to the north. The differences in the 850 hPa mean circulation for each of the models relative to ERA-Interim are plotted in Figure 1(b–k) and the mean northward flow between 120 and 150°E is given in Table 2 (fourth column, $V_{13.75S}$).

The NorESM1-M, CCSM4 and MIROC5 simulations all have cyclonic anomalies centred adjacent to the northwest Australian coast, which leads to northwesterly flow biases onto the continent (Figure 1(b–d) and Table 2, fourth column). Similarly, ACCESS1.3 and BNU-ESM have cyclonic anomalies close to northern Australia (Figure 1(e,f)) although the centres are located at 20°S, 140°E and 10°S, 120°E, respectively. The locations of the cyclonic anomalies in ACCESS1.3 and BNU-ESM cause anomalous northeasterly flow into the eastern and western halves of the continent, respectively. The BCC-CSM1-1-m, MRI-CGCM3, BCC-CSM1-1 and ACCESS1.0 (Figure 1(g–j) and Table 2, fourth column) models simulate either anomalous southeasterlies or southwesterlies over northern Australia, and IPSL-CM5A-LR (Figure 1(k)) has a strong easterly bias centred on approximately 10°S.

4.2. *Climatological vertical mass flux at 500 hPa*

The meridional mass flux (kg m^{-2}s^{-1}) at 500 hPa, calculated using the method in Schwendike *et al.* (2014), is plotted for the Australian region in Figure 5 to identify the strength of the local overturning circulation (termed the ψ-Hadley circulation by Schwendike *et al.*, 2014). The shading with solid white contours indicate a positive mass flux and upward motion and vice versa for the shading with dashed white contours. The solid black line in each figure marks the line of zero mass flux in the ERA-Interim reanalysis with the corresponding modelled zero mass flux contour dashed.

In NorESM1-M, CCSM4 and MIROC5, the region of positive mass flux extends further south by approximately 5° relative to ERA-Interim (Figure 5(b–d)). In ACCESS1.3, BNU-ESM, BCC-CSM1-1-m and MRI-CGCM3 the location of the zero mass flux contour lies within approximately 1° of the reanalysis estimate; however, the zero mass flux contour is slightly too far south in ACCESS1.3 and too far north in MRI-CGCM3, relative to ERA-Interim. BCC-CSM1-1 and ACCESS1.0 both have a large region of positive mass flux over northwest Australia, which is co-located with the centre of the heat low (section 4.3). Finally, the line separating positive and negative momentum fluxes is located approximately 2°–5° further north in IPSL-CM5A-LR than in ERA-Interim over northern Australia.

4.3. *Diurnal cycle*

The 925 hPa circulation over the continent is primarily easterly at 0800 AWST (Figure 6, first column), except in the north where there are westerlies associated with the residual cyclonic circulation around the nocturnal heat low. Likewise, at 0800 AWST the models have easterly flow over much of the land surface with cyclonic circulations in the northwest quadrant of the domain in Figure 6 (first column). There is also no evidence of strong convergence in the models (as in the reanalysis) at 0800 AWST.

By 1400 AWST, surface heating over the land (and therefore turbulence) has increased the low-level drag, weakening the 925 hPa winds and turning them cyclonically relative to 0800 AWST in the reanalysis (Figure 6, second column). Similarly, the 925 hPa flow weakens and turns cyclonically over the Australian land mass in each of the models between 0800 and 1400 AWST (Figure 6, second column). This indicates that the surface heating also increases the low-level friction in the models and compares well with the reanalysis, although the magnitude and direction of the actual flows in the models differ from the reanalysis.

By 2000 AWST there has been a reorganisation of the low-level flow relative to 1400 AWST in the reanalysis (compare the second and third columns in Figure 6). Surface cooling after sunset causes the nocturnal boundary layer to form, reducing the low-level drag and allowing the air to accelerate in towards the heat low centre producing strong convergence (Figure 6, third column, shaded region). This nocturnal rearrangement of the

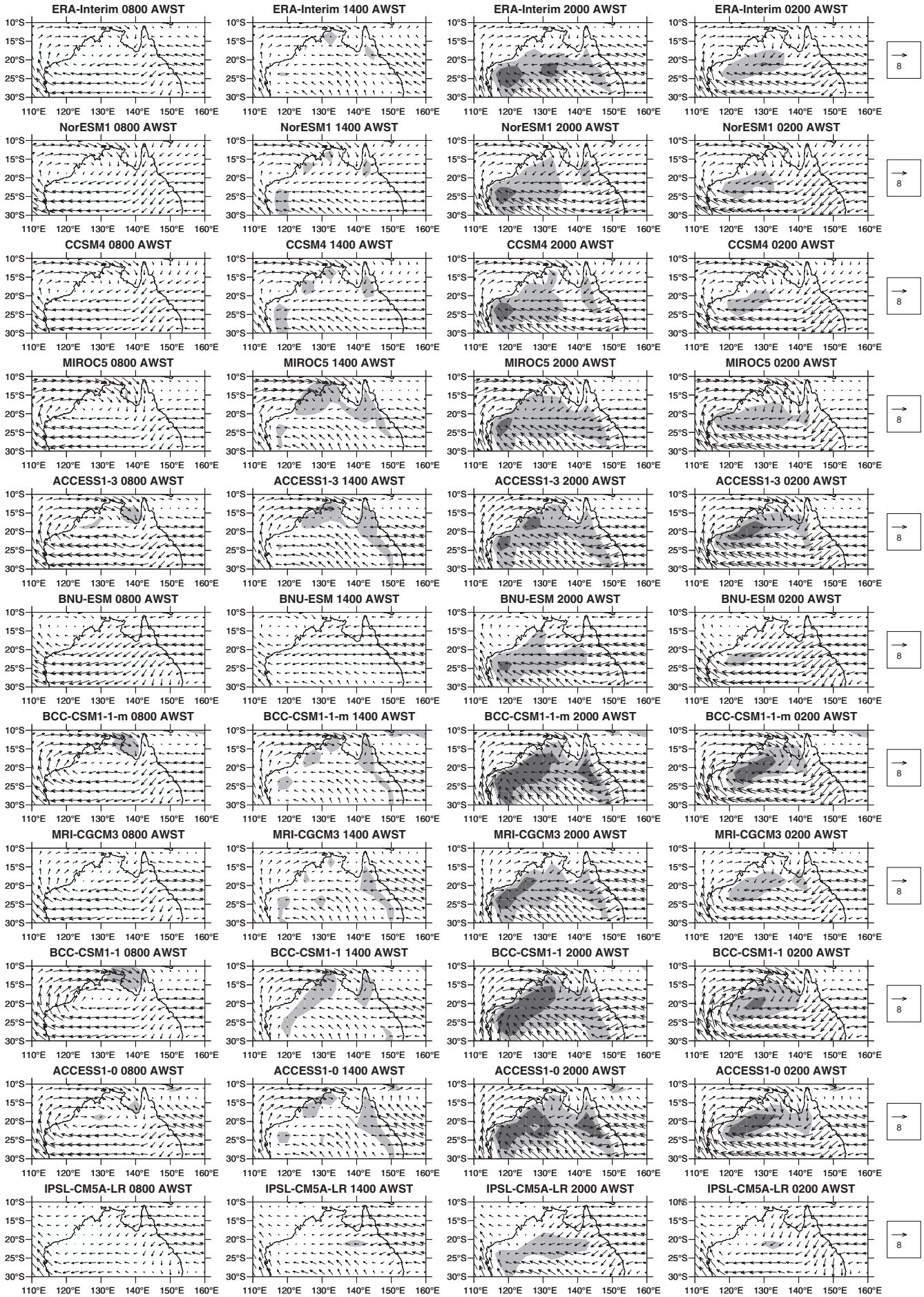

Figure 6. Composited DJF 925 hPa wind vectors ($m\,s^{-1}$, scale on the right hand side) from ERA-Interim (top row) and from each model (subsequent rows) at (column 1) 0800 AWST, (column 2) 1400 AWST, (column 3) 2000 AWST and (column 4) 0200 AWST. Shaded areas highlight regions where the convergence $\geq |5.0\times10^{-6}|\,s^{-1}$ (light) and $\geq |1.0\times10^{-5}|\,s^{-1}$ (dark).

flow over the Australian continent is a well-known feature of the summertime circulation (Racz and Smith, 1999; Spengler *et al.*, 2005; Arnup and Reeder, 2007, 2009; Berry *et al.*, 2011; Ackerley *et al.*, 2014). In comparison, the models also simulate strong convergence at 2000 AWST over northern Australia, although it is too strong in ACCESS1.0, BCC-CSM1-1 and BCC-CSM1-1-m and too weak in IPSL-CM5A-LR.

The 925 hPa flow turns anticyclonically between 2000 and 0200 AWST in the reanalysis as the flow reaches geostrophic balance and the convergence reduces as a result. The same process occurs in the models; however, both the flow and convergence are too strong in ACCESS1.0, ACCESS1.3, BCC-CSM1-1 and BCC-CSM1-1-m and too weak in IPSL-CM5A-LR.

5. Moisture transports and synoptic features that initiate rain

5.1. Back-trajectories at 850 hPa

Ten-day isobaric back-trajectories are calculated using the composited wind field in order to infer the moisture sources for rainfall *initiation* across northern Australia (following the method used in both Berry *et al.*, 2011; Ackerley *et al.*, 2014). Back-trajectories are produced at 850 hPa by compositing the wind field at that level on init and dry days (using AWAP and ERA-Interim, as described in section 2.2). The method is then applied to the models for their respective init and dry days.

The back trajectories are initiated from a specific grid point, therefore four points have been chosen across northern Australia that are considered to be representative of the precipitation and circulation characteristics in the models and observations. The first two points considered are located in eastern (eastern point, EP) and western (western point, WP) Australia where there are large biases in the modelled climatological rainfall (Figure 1 and Table 2). These two points also lie within the eastern and western rainfall peaks between 1100 and 1700 AWST and 1700 and 2300 AWST, respectively (Figure 4, discussed in section 3.3). The eastern point is located in the Great Dividing Range (marked by the square) and the western point lies within the Hamersley Ranges (marked by the triangle).

The third point (marked by a circle) lies within the Top End (TE) region of Australia, which is both near to the northernmost land extent of the Australian monsoon and another region where the models have opposing rainfall biases (Figure 1, Table 2). Finally, the fourth point (marked by the diamond shape) lies close to the southern boundary of the Australian monsoon rainfall (Figure 1) away from the coastline and is also located within the region of high nocturnal rainfall (Nocturnal Peak, NP) and convergence into the heat low (Figures 4 and 6, discussed in sections 3.3 and 4.3).

The calculated back-trajectories are plotted for the observations (ERA-Interim–AWAP; E-A in Figure 7) and each of the models (A to J, listed in Table 1) in Figure 7.

5.1.1. Eastern Point: EP

On init days, the air at 850 hPa originates from the east of the EP for ERA-Interim–AWAP (Figure 7(a)). The models all have similar back trajectories to ERA-Interim–AWAP, with the flow originating from the east of the continent.

On dry days (Figure 7(b)), the models simulate east-to-southeasterly flow, agreeing well with ERA-Interim–AWAP. The exceptions are ACCESS1.3 (B), ACCESS1.0 (A) and NorESM1-M (J), where the back trajectories originate from the northern Tasman Sea; nonetheless, the flow is easterly in those three models once the trajectories cross the east coast, which also occurs in all of the other models and ERA-Interim–AWAP.

5.1.2. Western Point: WP

The back-trajectories on the init days (Figure 7(c)) originate from the northeast coast of Australia in ERA-Interim–AWAP and all models except ACCESS1.0 (A) and BCC-CSM1-1 (C). Therefore the moisture source is primarily from the Coral Sea and the Gulf of Carpentaria (except in ACCESS1.0 (A) and BCC-CSM1-1 (C), where parcels originate from southeast Australia).

On dry days, the back-trajectories approach the WP from the east to southeast, indicating that the air parcels originate over the land surface and are therefore drier (Figure 7(d)).

5.1.3. Top End: TE

The back-trajectories on init and dry days at the TE point are plotted in Figure 7(e,f), respectively. The ERA-Interim–AWAP trajectory crosses the Gulf of Carpentaria, the Cape York Peninsula and originates over the Coral Sea on init days, which is also the case in the BCC-CSM1-1 (C) and MIROC5 (H) models. Both CCSM4 (F) and NorESM1-M (J) have trajectories that circulate cyclonically towards the TE point for init days relative to dry days. The trajectories for ACCESS1.0 (A) and ACCESS1.3 (B) originate from over the continent to the south and east of TE. The trajectories in the other models (BCC-CSM1-1-m (D), BNU-ESM (E), IPSL-CM5A-LR (G) and MRI-CGCM3 (I)) extend toward the edge of the domain, which is indicative of strong easterly flow. The dry days are very similar across the models and ERA-Interim–AWAP with eastsoutheasterly flow.

5.1.4. Nocturnal Peak: NP

At NP, in all cases (ERA-AWAP and models), the back-trajectories arrive from the east to northeast on init days (Figure 7(g)) and from the east to south-east on dry days (Figure 7(h)).

From the back-trajectories on init days (Figure 7(g)), the models can be split into three groups:

Group 1: ACCESS1.0 (A), BCC-CSM1-1 (C) and BCC-CSM1-1-m (D) have back-trajectories that originate from the northwest of the continent.

Group 2: The back-trajectories in ACCESS1.3 (B), BNU-ESM (E), IPSL-CM5A-LR (G) and MRI-CGCM3 (I) originate over the northern Coral Sea and agree well with ERA-Interim–AWAP.

Group 3: The trajectories in CCSM4 (F), MIROC5 (H) and NorESM1-M (J) originate from the southern Maritime Continent.

On dry days the back-trajectories in all models traverse a larger proportion of the Australian continent.

5.2. Synoptic circulation for initiating rain

Previous work by Hung and Yanai (2004), Davidson *et al.* (2007), Wheeler *et al.* (2009), Risbey *et al.* (2011), Berry *et al.* (2011, 2012), and Lin and Li (2012) have all shown that coherent synoptic circulation features (such as extratropical Rossby wave activity) at mid-to-upper levels of the troposphere (around 500 to 200 hPa) can be responsible for initiating rain over northern and central Australia. The circulation features induce northerly, onshore flow at mid-levels (500 hPa), which brings moist, tropical air onto the continent causing rain. Therefore, the differences in the geopotential heights and wind fields at 500 hPa between init and dry days at EP, WP, TE and NP are assessed in this section (Figure 8).

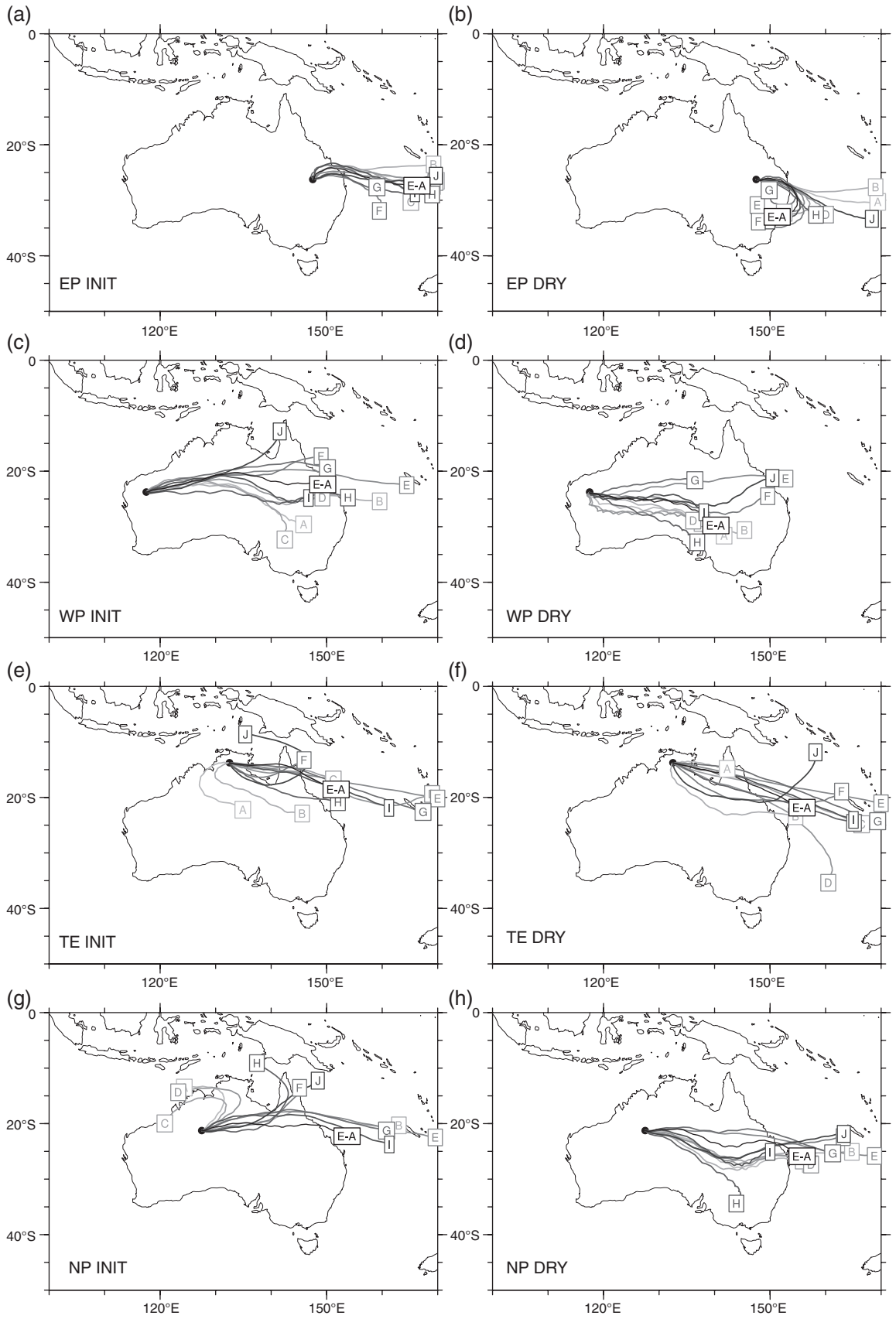

Figure 7. Ten-day back-trajectories along the 850 hPa surface starting at the Eastern Point (EP) on (a) init days and (b) dry days from ERA-Interim–AWAP (E-A) and from each of the models A to J (listed in Table 1). Equivalent composites for init and dry conditions are also plotted for (c, d) the Western Point (WP), (e, f) Top End (TE) and (g, h) the Nocturnal Peak (NP).

5.2.1. EP

There are negative geopotential height and northwesterly flow anomalies centred on southeast Australia, which extend from approximately 60 to 20°S in ERA-AWAP and all models (Figure 8, first column). The height and wind anomaly fields resemble an 'easterly dip' (Fandry and Leslie, 1984; Adams, 1986), which is a common feature of the summertime circulation in eastern Australia and is known to be associated with rainfall. There are also positive height anomalies to the the southwest and northeast of the negative anomaly. All of the models resemble the ERA-Interim circulation and geopotential height field, which indicates

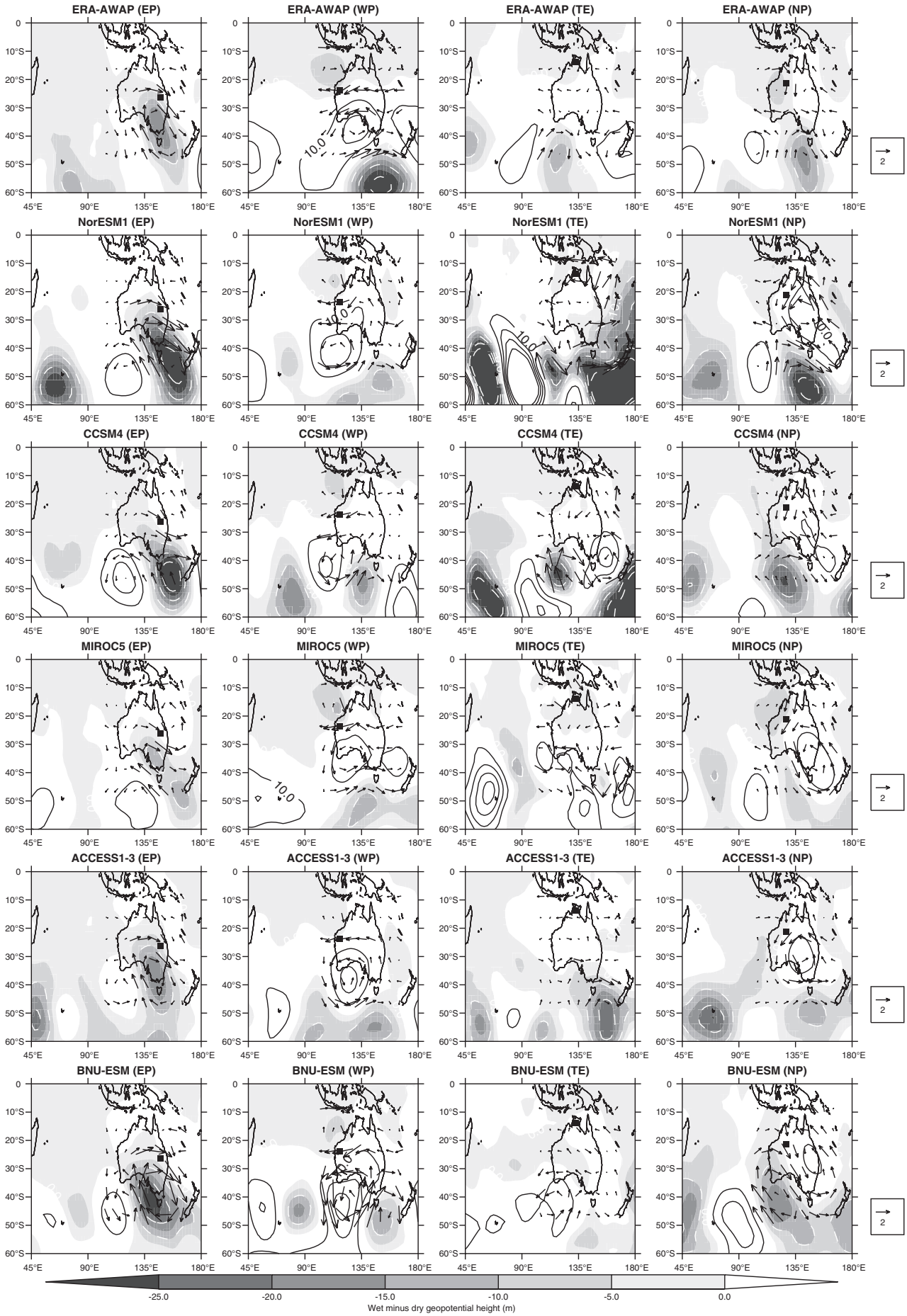

Figure 8. Composited geopotential height (m) and wind vector ($m\,s^{-1}$, scale on the right-hand side) anomalies at 500 hPa for init minus dry days at (column 1) EP, (column 2) WP, (column 3) TE and (column 4) NP in the ERA-Interim-AWAP data (top row) and each model (subsequent rows). Geopotential height anomalies are shown by shaded white dashed contours for negative values and unshaded solid black contours for positive values (interval 5 m).

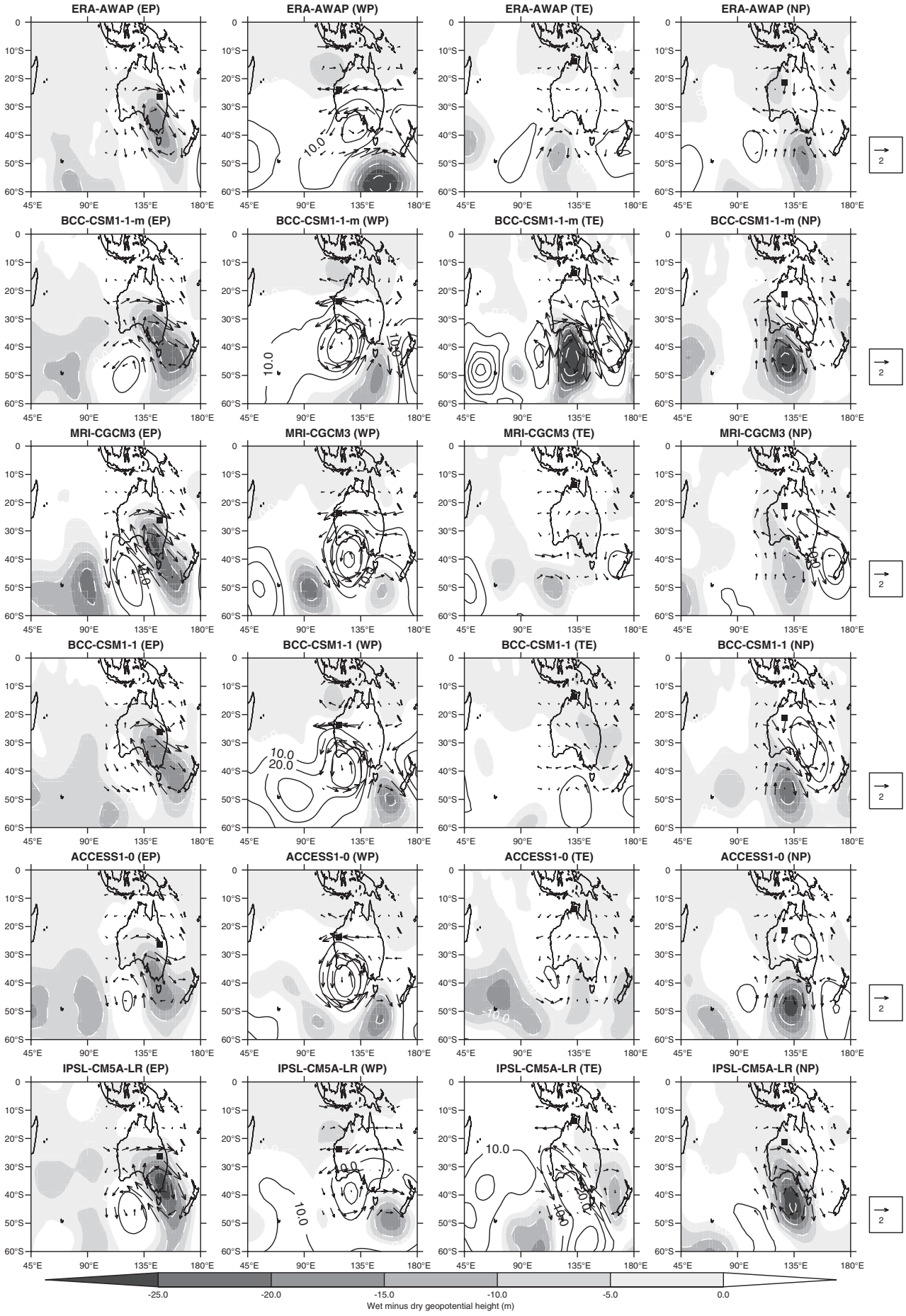

Figure 8. Continued.

that the conditions for the initiation of precipitation in the models are very similar to those in the observations.

5.2.2. WP

There is a strong positive geopotential height anomaly centred to the south of Australia in the observations with negative anomalies to the northwest and southeast, which cause anomalous northeasterlies over northern Australia (Figure 8, second column). This pattern appears to resemble the flow during phase 5 of the MJO (Wheeler *et al.*, 2009, their Figure 8) when precipitation is high in this region. The models also resemble this pattern with negative anomalies in the Tropics to the northwest of Australia and a positive anomaly to the south.

5.2.3. TE

The TE composites, unlike EP and WP, show no strong evidence of Extratropical–Tropical interaction; however, there are positive and negative geopotential height anomalies between 40 and 60°S, indicating that there may be wave activity in the Extratropics when precipitation is initiated (Figure 8, third column). The model composites are very different from each other and the observations, which suggests that the circulation structures which initiate precipitation at TE are not represented well by the models or that they are of secondary importance to other initiation processes such as local convection.

5.2.4. NP

At NP, there is a negative geopotential height anomaly over northwest Australia with onshore flow, which appears to be linked to a negative anomaly in the extratropics (Figure 8, fourth column). The figure resembles the anomalous circulation patterns for initiating rainfall in this region shown by Hung and Yanai (2004) and Berry *et al.* (2011). Moreover, the circulation resembles the one identified by Wheeler *et al.* (2009) (their Figure 8) in phases 3 and 4 of the MJO where the interaction between a midlatitude wave train and the MJO initiates rainfall over the Australian continent ahead of the main region of tropical convection. The models also produce a similar feature in all cases, with a northwest to southeast trough extending from around 20 to 60°S.

6. Discussion

This study documents the precipitation and circulation patterns and moisture transports over northern Australia during the summer in the observations and a selection of GCMs from the CMIP5 archive. The salient features of those circulation and moisture transport patterns are now discussed and are connected with the precipitation biases where relevant.

6.1. The diurnal cycle

The diurnal cycle of the circulation in each model compares well with ERA-Interim in that:

1. the flow weakens and turns cyclonically over the land from the early morning to the afternoon due to the increased surface drag from solar heating and convection;
2. the flow initially accelerates towards the centre of the heat low over the land (around 2000 AWST) as the stable nocturnal boundary layer reduces the low-level friction, which causes the strong convergence. The flow then turns anticyclonically between 2000 and 0200 AWST as the flow reaches geostropic balance and the convergence reduces.

Conversely, the timing of precipitation is poorly represented as the simulated convection develops too early in the day –although all models (except IPSL-CM5A-LR) produce nocturnal rainfall over the continent due to the increased convergence.

6.2. Low-level circulation and moisture transport

Four of the five models wetter than CMAP north of 30°S have mean northerly flow at 850 hPa between 120 and 150°E (NorESM1-M, CCSM4, MIROC5 and BNU-ESM; Table 2, fourth column). Conversely, four of the five driest models have southerlies between 120 and 150°E (BCC-CSM1-1-m, MRI-CGCM3, BCC-CSM1-1 and ACCESS1.0; Table 2, fourth column). This result suggests that systematic errors in the low-level circulation may provide the necessary moisture for the simulated rainfall biases over northern Australia.

These moisture sources are evaluated further in the 10 day back-trajectories (section 5.1). In eastern Australia (at EP) the low-level moisture required to initiate rain is supplied from the Tasman Sea (to the east of Australia) in all models, which agrees with the observations (Figure 7(a)), although there is no clear separation between the wetter and drier models. Nonetheless, by comparing Figure 2(b,k), it can be seen that the frequency of rain at EP in the wettest model is higher than that in the driest model (NorESM1-M and IPSL-CM5A-LR, respectively; Table 2, fifth column), which suggests that moisture transport from the Tasman Sea occurs more often in the wetter models than the drier ones at this point.

Nonetheless, as discussed above, the four wettest models in the east (ACCESS1.3, CCSM4, MIROC5 and NorESM1-M; Table 2, fifth column) also have anomalous northerly onshore flow (Figure 1) and higher frequencies of precipitation than the observations (Figure 2).

In the west of Australia (WP) there is a clear separation between the moisture sources for the wettest and driest models (NorESM1-M and BCC-CSM1-1; Figure 7(c) and Table 2, sixth column). The back-trajectory in the NorESM1-M simulation on wet days originates from the ocean in Gulf of Carpentaria (to the northeast of WP) whereas the trajectory for BCC-CSM1-1 originates from over the drier continental interior (to the southeast). Similarly, the models with the highest rainfall at the NP point (NorESM1-M, CCSM4 and MIROC5) have back-trajectories that originate from southern Papua New Guinea (to the north of NP) whereas the back-trajectories in the two driest models (ACCESS1.0 and BCC-CSM1-1) originate from over the continent to the southwest (Figure 7(e) and Table 2, eighth column).

At the TE of Australia, the back trajectories change little between wet and dry days, which implies that the larger-scale circulation may be of less importance for the initiation of rainfall (this point is adjacent to the coast). For example, IPSL-CM5A-LR simulates the driest conditions of the models evaluated here at TE although the calculated back-trajectories originate from over the Coral Sea and is the case for the other models.

6.3. Tropical–extratropical interaction

There is evidence for the interaction of tropical and extratropical, mid-level (500 hPa) circulation features that are responsible for initiating rain over northern Australia in the observations and all models. These can be seen in Figure 8 at:

1. EP: a midlatitude trough interacting with an easterly dip.
2. WP: an anomalous anticyclone over southern Australia, which lies between a trough to the northwest and southeast and resembles phase 5 of the MJO (Wheeler *et al.*, 2009, their Figure 8).
3. NP: a midlatitude Rossby wave train with a trough extending over northwest Australia into the Tropics, which resembles phases 3 and 4 of the MJO (Wheeler *et al.*, 2009, their Figure 8).

However there is little evidence of any organised tropical or extratropical system being responsible for initiating rain at TE. Moreover, there is no consensus in the anomalous geopotential height and flow fields at 500 hPa for models with a wet or dry bias at TE, which provides further evidence that the modelled precipitation is unlikely to be controlled by the large-scale circulation.

6.4. Parametrizations of convection and vertical mass flux

The model simulations with the highest positive precipitation biases (CCSM4, MIROC5 and NorESM1-M) have higher frequencies of rainfall days (and convective rainfall) than CMORPH and higher daily mean rain accumulations than the other models (Figures 2 and 3). Furthermore, the region of positive mass flux at 500 hPa extends further south (by almost 5°) in CCSM4, MIROC5 and NorESM1-M (Figure 5(b–d)), which suggests these models simulate frequent convection (and vertical ascent) in this region. Gent *et al.* (2011) state that for CCSM4: 'Changes were made to the deep convection scheme... [which] resulted in a much improved representation of deep convection that occurs considerably less frequently, but is much more intense'. These changes may therefore be contributing to the the positive (upward) mass flux over northern Australia. As both CCSM4 and NorESM1-M use the same atmospheric model (CAM4) and only differ in their representation of aerosol (Bentsen *et al.*, 2013), it is unsurprising that they both have positive rainfall biases over Australia in summer (when convection is at its strongest). Similarly, Watanabe *et al.* (2010) state that: 'global mean precipitation is excessive in MIROC5, suggesting a hydrological cycle that is too active'. This statement is consistent with the local positive mass flux given in Figure 5(d). Therefore, in CCSM4, MIROC5 and NorESM1-M it appears that precipitation is initiated under the correct synoptic conditions; however, once the precipitation is initiated, the convection scheme may be causing the positive mass flux biases that result both in the rainfall errors and the low-level flow anomalies at 850 hPa (Figure 1(b–d)).

BNU-ESM simulates too much precipitation over much of the Australian continent with rainfall that is too frequent (Figures 1(f) and 2(f)). Notably, a similar atmospheric module to the one used in CCSM4 (CAM4) is used in BNU-ESM (CAM3.5; Ji *et al.*, 2014). The positive rainfall biases over northern Australia in BNU-ESM may therefore be caused by the representation of convection (in a similar way to the errors in CCSM4 and NorESM1-M). Nonetheless, the daily mean rainfall in BNU-ESM is lower than in both CCSM4 and NorESM1-M, and the precipitation biases are equally likely to be due to differences in the representation of other earth-system processes (such as the land surface scheme).

The IPSL-CM5A-LR model has the lowest simulated rainfall northward of 30°S over Australia (Table 2) with the contour separating the positive and negative climatological mass flux located 2–5° further north than in ERA-Interim (Figure 5(k)). Nonetheless, the frequency of precipitation (and convective precipitation) is much higher than in CMORPH (compare Figure 2(a,k)) although the mean daily rainfall is much lower than CMORPH (compare Figure 3(a, k)). The diurnal cycle of precipitation simulated by IPSL-CM5A-LR is particularly poor (Figure 4, bottom row), with convection initiated too early in the day and very little rainfall ($\leq$15% of the daily mean) after 1700 AWST. These results suggest that the convection in IPSL-CM5A-LR triggers too easily but does not transport enough mass vertically relative to the reanalysis. Nonetheless, the circulation features for initiating rainfall over northern Australia are represented by IPSL-CM5A-LR (Figure 8), reinforcing the idea that the representation of convection may be the primary cause of the dry bias. Indeed, Dufresne *et al.* (2013) show that increasing the resolution alone in IPSL-CM5A does not improve the representation of tropical rainfall; it is only when the convection scheme is changed (IPSL-CM5B; Hourdin *et al.*, 2013) that there is improvement.

ACCESS1.0 and BCC-CSM1-1 (the next two driest models over northern Australia after IPSL-CM5A-LR, Table 2) both have strong, positive mass fluxes over northwest Australia (Figure 5(i,j)), which coincide with very strong nocturnal convergence into their simulated heat lows (Figure 6). Therefore, the strong positive mass flux over northwest Australia is likely to be associated with the heat low being too vigorous, which is a problem that is also common to West Africa in GCM simulations with parametrized convection (Garcia-Carreras *et al.*, 2013; Marsham *et al.*, 2013; Birch *et al.*, 2014). The intensity of precipitation in these models is weaker than in CMORPH although the frequency of precipitation is similar, which may be due to the drier low-level air circulating from the Australian continent (as seen in the back-trajectory analysis in Figure 7(g)). The vertical mass flux in the heat low simulated by BCC-CSM1-1-m is similar in extent to ACCESS1.0; however, the dry bias in BCC-CSM1-1-m is primarily restricted to the western half of the continent and the anomalous southwesterlies along the coast of northwest Australia are weaker.

The location of the boundary between positive and negative vertical mass fluxes is slightly further north in MRI-CGCM3 relative to ERA-Interim (Figure 5(h)). The frequency of precipitation is overestimated slightly (by approximately 10%) in MRI-CGCM3 relative to CMORPH, but the daily mean accumulation is underestimated (by approximately 3–6 mm day^{-1}) relative to CMORPH (Figures 2 and 3). Again, it appears that the vertical mass flux from convection may be underestimated relative to the observations, which results in the negative precipitation bias in MRI-CGCM3.

As for ACCESS1.3, there are two main differences relative to ACCESS1.0 which may be responsible for the differences in their simulated rainfall:

1. the inclusion of the CABLE surface scheme (Kowalczyk *et al.*, 2006);
2. the inclusion of the PC2 cloud scheme (Wilson *et al.*, 2008a; Franklin *et al.*, 2012)

It is likely to be either or both of these changes that cause the wet bias in eastern Australia relative to ACCESS1.0. Nonetheless, the PC2 scheme (used in ACCESS1.3 but not ACCESS1.0) includes a representation of the detrainment of convectively produced condensate into the large-scale cloud scheme, which increases the amount of large-scale (non-convective) precipitation (Wilson *et al.*, 2008b) and possibly increase the overall (convective plus large-scale) rainfall. The higher rainfall rates in ACCESS1.3 relative to ACCESS1.0 may therefore result from the change in the parametrized convection scheme when PC2 is used.

7. Conclusions

The aims of this article are to document and better understand the modelled summertime precipitation characteristics over northern Australia in the CMIP5 GCMs, from the diurnal cycle to the seasonal mean, and to identify whether the circulation characteristics and moisture transports responsible for initiating that rainfall are comparable to the observations.

This study has shown that:

- Four of the five wettest simulations of northern Australian rainfall have mean northerly flow between 120 and 150°E and, conversely, four of the five driest models have mean southerly flow across the same longitudes, suggesting that the modelled precipitation biases are linked to the meridional circulation at 850 hPa (Table 2).
- The model with the lowest simulated rainfall over northern Australia (IPSL-CM5A-LR) produces weak mean northerly flow into northern Australia at 850 hPa (Table 2); however, the vertical mass flux (Figure 5(k)) and precipitation intensities (Figure 3(k)) are much weaker than in the reanalysis, which indicates that weak convection may be the primary cause of the negative precipitation error.
- Conversely, the three wettest models (NorESM1-M, CCSM4 and MIROC5; Table 2) have the most active convective precipitation of all the models, therefore the strength of the local convection may be responsible for maintaining the low-level northerlies, which bring further moisture onto the continent for precipitation.
- There is evidence that mid-level (500 hPa) synoptic features identified in the observations are responsible for *initiating* rainfall over western, central and eastern Australia in the models; however,

there is little consensus across the models and observations as to whether any mid-level disturbances initiate rainfall over northern Australia (Figure 8).

- There is no evidence that the mid-level circulation features responsible for initiating rainfall are the cause of the simulated precipitation biases, especially given the strong agreement in the flow and geopototential height anomaly fields at 500 hPa for three of the four grid points considered.
- The diurnal cycle of precipitation is dominated by the early triggering of convection, which is approximately 3–6 h too early relative to the observations (Figure 4); however, the diurnal cycle of the circulation over Australia at 925 hPa is represented well by the models relative to the reanalysis (Figure 6).
- As with the large-scale flow anomalies at 500 hPa, the diurnal cycle of the circulation and precipitation cannot be used directly to identify models with positive or negative rainfall biases over northern Australia.

Given that these models are routinely used as tools to project future rainfall in this region, it is important to know whether the processes that lead to rainfall are represented well and, if they are not, to identify which of the processes is the main cause of error (and over what time-scale). This study has shown that the systems responsible for *initiating* rainfall are represented well in these models; however, it is the response of the simulated convection to those initiation processes that is likely to be the cause of the precipitation biases described.

Acknowledgements

The authors would like to thank the Australian National Computational Infrastructure National Facility and the Earth System Grid Federation (2013–2014) for providing the model data. AWAP data were provided by the Australian BoM, ERA-Interim data were provided by the ECMWF and the CMORPH rainfall data were provided by UCAR at https://climatedataguide.ucar.edu/climate-data/cmorph-cpc-morphing-technique-high-resolution-precipitation-60s-60n. CMAP Precipitation data were provided by the NOAA/OAR/ESRL PSD, Boulder, Colorado, USA, from their web site at http://www.esrl.noaa.gov/psd/. This work was funded by the Australian Research Council grant DP0985665, 'Rainfall over the Maritime Continent and Northern Australia'.

References

Ackerley D, Berry G, Jakob C, Reeder MJ. 2014. The roles of diurnal forcing and large-scale moisture transport for initiating rain over northwest Australia in a GCM. *Q. J. R. Meteorol. Soc.*, doi: 10.1002/qj.2316.

Adams M. 1986. A theoretical study of the inland trough of northeastern Australia. *Aust. Meteorol. Mag.* **34**: 85–92.

Arnup SJ, Reeder MJ. 2007. The diurnal and seasonal variation of the northern Australian dryline. *Mon. Weather Rev.* **135**: 2995–3008.

Arnup SJ, Reeder MJ. 2009. The structure and evolution of the northern Australian dryline. *Aust. Meteorol. Oceanogr. J.* **58**: 215–231.

Bentsen M, Bethke I, Debernard JB, Iversen T, Kirkevåg A, Seland Ø, Drange H, Roelandt C, Seierstad IA, Hoose C, Kristjánsson JE. 2013. The Norwegian Earth System Model, NorESM1-M Part 1: Description and basic evaluation of the physical climate. *Geosci. Model Dev.* **6**: 687–720, doi: 10.5194/gmd-6-687-2013.

Berry G, Reeder MJ, Jakob C. 2011. Physical mechanisms regulating summertime rainfall over northwestern Australia. *J. Clim.* **24**: 3705–3717.

Berry GJ, Reeder MJ, Jakob C. 2012. Coherent synoptic disturbances in the Australian monsoon. *J. Clim.* **25**: 8409–8421.

Bi D, Dix M, Marsland SJ, O'Farrell S, Rashid HA, Uotila P, Hirst AC, Golebiewski EKM, Sullivan A, Yan H, Hannah N, Franklin C, Sun Z, Vohralik P, Watterson I, Zhou Z, Fiedler R, Collier M, Ma Y, Noonan J, Stevens L, Uhe P, Zhu H, Griffies SM, Hill R, Harris C, Puri K. 2013. The ACCESS coupled model: Description, control climate and evaluation. *Aust. Meteorol. Oceanogr. J.* **63**: 41–64.

Birch CE, Parker DJ, Marsham JH, Copsey D, Garcia-Carreras L. 2014. A seamless assessment of the role of convection in the water cycle of the West African Monsoon. *J. Geophys. Res.* **119**: 2890–2912, doi: 10.1002/2013JD020887.

Brown JR, Jakob C, Haynes JM. 2010. An evaluation of rainfall frequency and intensity over the Australian region in a global climate model. *J. Clim.* **23**: 6504–6525.

Dai A. 2006. Precipitation characteristics in eighteen coupled climate models. *J. Clim.* **19**: 4605–4630.

Dai A, Trenberth KE. 2004. The diurnal cycle and its depiction in the community climate system model. *J. Clim.* **17**: 930–951.

Dai A, Lin X, Hsu KL. 2007. The frequency, intensity, and the diurnal cycle of precipitation in surface and satellite observations over low- and mid-latitudes. *Clim. Dyn.* **29**: 727–744.

Davidson NE, Tory KJ, Reeder MJ, Drosdowsky WL. 2007. Extra-tropical–tropical interaction during onset of the Australian monsoon: Reanalysis, diagnostics and idealized dry simulations. *J. Atmos. Sci.* **64**: 3475–3498.

Dee DP, Uppala SM, Simmons AJ, Berrisford P, Poli P, Kobayashi S, Andrae U, Balmaseda MA, Balsamo G, Bauer P, Bechtold P, Beljaars ACM van de Berg L, Bidlot J, Bormann N, Delsol C, Dragani R, Fuentes M, Geer AJ, Haimberger L, Healy SB, Hersbach H, Holm EV, Isaksen L, Kallberg P, Kohler M, Matricardi M, McNally AP, Monge-Sanz BM, Morcrette J-J, Park BK, de Rosnay CPP, Tavolato C, Thepaut J-N, Vitart F. 2011. The ERA-Interim reanalysis: Configuration and performance of the data assimilation system. *Q. J. R. Meteorol. Soc.* **137**: 553–597.

Dufresne JL, Foujols MA, Denvil S, Caubel A, Marti O, Aumont O, Balkanski Y, Bekki S, Bellenger H, Benshila R, Bony S, Bopp L, Braconnot P, Brockmann P, Cadule P, Cheruy F, Codron F, Cozic A, Cugnet D, Noblet N, Duvel JP, Ethé C, Fairhead L, Fichefet T, Flavoni S, Friedlingstein P, Grandpeix JY, Guez L, Guilyardi E, Hauglustaine D, Hourdin F, Idelkadi A, Ghattas J, Joussaume S, Kageyama M, Krinner G, Labetoulle S, Lahellec A, Lefebvre MP, Lefevre F, Levy C, Li Z, Lloyd J, Lott F, Madec G, Mancip M, Marchand M, Masson S, Meurdesoif Y, Mignot J, Musat I, Parouty S, Polcher J, Rio C, Schulz M, Swingedouw D, Szopa S, Talandier C, Terray P, Viovy N, Vuichard N. 2013. Climate change projections using the IPSL-CM5 Earth System Model: From CMIP3 to CMIP5. *Clim. Dyn.* **40**: 2123–2165, doi: 10.1007/s00382-012-1636-1.

Fandry CB, Leslie LM. 1984. A two-layer quasi-geostrophic model of summertime trough formation in the Australian subtropical easterlies. *J. Atmos. Sci.* **41**: 804–818.

Franklin CN, Jakob C, Dix M, Protat A, Roff G. 2012. Assessing the performance of a prognostic and a diagnostic cloud scheme using single-column model simulations of TWP–ICE. *Q. J. R. Meteorol. Soc.* **138**: 734–754.

Garcia-Carreras L, Marsham JH, Parker DJ, Bain CL, Milton S, Saci A, Salah-Ferroudj M, Ouchene B, Washington R. 2013. The impact of convective cold pool outflows on model biases in the Sahara. *Geophys. Res. Lett.* **40**: 1647–1652, doi: 10.1002/grl.50239.

Gates WL. 1992. AMIP: The atmospheric model intercomparison project. *Bull. Am. Meteorol. Soc.* **73**: 1962–1970.

Gates WL, Boyle JS, Covey C, Dease CG, Doutriaux CM, Drach RS, Florino M, Gleckler PJ, Hnilo JJ, Marlais SM, Phillips TJ, Potter GL, Santer BD, Sperber KR, Taylor KE, Williams DN. 1999. An overview of the results of the atmospheric model intercomparison project (AMIP I). *Bull. Am. Meteorol. Soc.* **80**: 29–55.

Gent PR, Danabasoglu G, Donner LJ, Holland MM, Hunke EC, Jayne SR, Lawrence DM, Neale RB, Rasch PJ, Vertenstein M, Worley PH, Yang ZL, Zhang M. 2011. The Community Climate System Model Version 4. *J. Clim.* **24**: 4973–4991.

Grose MR, Brown JN, Narsey S, Brown JR, Murphy BF, Langlais C, Gupta AS, Moise AF, Irving DB. 2014. Assessment of the CMIP5 global climate model simulations of the western tropical Pacific climate system and comparison to CMIP3. *Int. J. Climatol.* **34**: 3382–3399, doi: 10.1002/joc.3916.

Hewitt HT, Copsey D, Culverwell ID, Harriss CM, Hill RSR, Keen AB, McLaren AJ, Hunke EC. 2011. Design and implementation of the infrastructure of HadGEM3: The next-generation Met Office climate modelling system. *Geosci. Model Dev.* **4**: 223–253.

Hourdin F, Grandpeix JY, Rio C, Bony S, Jam A, Cheruy F, Rochetin N, Fairhead L, Idelkadi A, Musat I, Dufresne JL, Lahellec A, Lefebvre M, Roehrig R. 2013. Lmdz5b: The atmospheric component of the IPSL climate model with revisited parameterizations for clouds and convection. *Clim. Dyn.* **40**: 2193–2222, doi: 10.1007/s00382-012-1343-y.

Hung CW, Yanai M. 2004. Factors contributing to the onset of the Australian summer monsoon. *Q. J. R. Meteorol. Soc.* **130**: 739–758.

Irving DB, Perkins SE, Brown JR, Gupta AS, Moise AF, Murphy BF, Muir LC, Colman RA, Power SB, Delage FP, Brown JN. 2011. Evaluating global climate models for the Pacific island region. *Clim. Res.* **49**: 169–187.

Ji D, Wang L, Feng J, Wu Q, Cheng H, Zhang Q, Yang J, Dong W, Dai Y, Gong D, Zhang RH, Wang X, Liu J, Moore JC, Chen D, Zhou M. 2014. Description and basic evaluation of Beijing Normal University Earth System Model (BNU-ESM) version 1, *Geosci. Model Dev.* **7**: 2039–2064, doi: 10.5194/gmd-7-2039-2014.

Jones DA, Wang W, Fawcett R. 2009. High-quality spatial climate data-sets for Australia. *Aust. Meteorol. Oceanogr. J.* **58**: 233–248.

Joyce RJ, Janowiak JE, Arkin PA, Xie P. 2004. CMORPH: A method that produces global precipitation estimates from microwave and infrared data at high spatial and temporal resolution. *J. Hydrometeorol.* **5**: 487–503.

Keenan TD, Carbone RE. 2008. Propagation and diurnal evolution of warm season cloudiness in the Australian and Maritime Continent region. *Mon. Weather Rev.* **136**: 973–994.

Klingaman NP, Woolnough SJ, Syktus J. 2012. On the drivers of interannual variability and decadal rainfall variability in Queensland, Australia. *Q. J. R. Meteorol. Soc.* **33**: 2413–2430, doi: 10.1002/joc.3593.

Kowalczyk EA, Wang YP, Law RM, Davies HL, McGregor JL, Abramowitz G. 2006. 'The CSIRO atmosphere biosphere land exchange (CABLE) model for use in climate models and as an offline model', Marine and Atmospheric Research paper 013. CSIRO: Aspendale, Australia.

Kowalczyk EA, Stevens L, Law RM, Dix M, Wang YP, Harman IN, Haynes K, Srbinovsky J, Pak B, Ziehn T. 2013. The land surface model component of access: Description and impact on simulated surface climatology. *Aust. Meteorol. Oceanogr. J.* **63**: 65–82.

Lin Z, Li Y. 2012. Remote influence of the Tropical Atlantic on the variability and trend in northwest Australia summer rainfall. *J. Clim.* **25**: 2408–2420.

Marsham JH, Dixon NS, Garcia-Carreras L, Lister GMS, Parker DJ, Knippertz P, Birch CE. 2013. The role of moist convection in the West African monsoon system: Insights from continental-scale convection-permitting simulations. *Geophys. Res. Lett.* **40**: 1843–1849, doi: 10.1002/grl.50347.

Martin GM, Bellouin N, Collins WJ, Culverwell ID, Halloran PR, Hardiman SC, Hinton TJ, Jones CD, McDonald RE, McLaren AJ, O'Connor FM, Roberts MJ, Rodriguez JM, Woodward S, Best MJ, Brooks ME, Brown AR, Butchart N, Dearden C, Derbyshire SH, Dharssi I, Doutriaux-Boucher M, Edwards JM, Falloon PD, Gedney N, Gray LJ, Hewitt HT, Hobson M, Huddleston MR, Hughes J, Ineson S, Ingram WJ, James PM, Johns TC, Johnson CE, Jones A, Jones CP, Joshi MM, Keen AB, Liddicoat S, Lock AP, Maidens AV, Manners JC, Milton SF, Rae JGL, Ridley JK, Sellar A, Senior CA, Totterdell IJ, Verhoef A, Vidale PL, Wiltshire A. 2011. The HadGEM2 family of Met Office Unified Model climate configurations. *Geosci. Model Dev.* **4**: 723–757, doi: 10.5194/gmd-4-723-2011.

Racz Z, Smith RK. 1999. The dynamics of heat lows. *Q. J. R. Meteorol. Soc.* **125**: 225–252.

Risbey JS, McIntosh PC, Pook MJ, Rashid HA, Hirst AC. 2011. Evaluation of rainfall drivers and teleconnections in an ACCESS AMIP run. *Aust. Meteorol. Oceanogr. J.* **61**: 91–105.

Schwendike J, Govekar P, Reeder MJ, Wardle R, Berry GJ, Jakob C. 2014. Local partitioning of the overturning circulations in the Tropics and the connection to the Hadley and Walker circulations. *J. Geophys. Res.* **119**: 1322–1339, doi: 10.1002/2013JD020742.

Spengler T, Reeder MJ, Smith RK. 2005. The dynamics of heat lows in simple background flows. *Q. J. R. Meteorol. Soc.* **19**: 3147–3165.

Stephens GL, L'Ecuyer T, Forbes R, Gettlemen A, Golaz JC, Bodas-Salcedo A, Suzuki K, Gabriel P, Haynes J. 2010. Dreary state of precipitation in global models. *J. Geophys. Res.* **115**: D24211, doi:10.1029/2010JD014532.

Stratton RA, Stirling AJ. 2012. Improving the diurnal cycle of convection in GCMs. *Q. J. R. Meteorol. Soc.* **138**: 1121–1134.

Sun Y, Solomon S, Dai A, Portmann RW. 2006. How often does it rain? *J. Clim.* **19**: 916–934.

Suppiah R. 1992. The Australian summer monsoon: A review. *Prog. Phys. Geog.* **16**: 283–318.

Taylor KE, Williamson D, Zwiers F. 2000. 'The sea surface temperature and sea-ice concentration boundary conditions of AMIP II simulations', PCMDI report 60. Lawrence Livermore National Laboratory: Livermore, CA.

Taylor K, Stouffer RJ, Meehl GA. 2012. An overview of CMIP5 and the experiment design. *Bull. Am. Meteorol. Soc.* **93**: 485–498.

Watanabe M, Suzuki T, O'Ishi R, Komuro Y, Watanabe S, Emori S, Takemura T, Chikira M, Ogura T, Sekiguchi M, Takata K, Yamazaki S, Yokohata T, Nozawa T, Hasumi H, Tatebe H, Kimoto M. 2010. Improved climate simulation by MIROC5: Mean states, variability and climate sensitivity. *J. Clim.* **23**: 6312–6335.

Wheeler MC, Hendon HH, Cleland S, Meinke H, Donald A. 2009. Impacts of the Madden–Julian Oscillation on Australian rainfall and circulation. *J. Clim.* **22**: 1482–1498.

Wilson DR, Bushell AC, Kerr-Munslow AM, Price D, Morcrette C. 2008a. PC2: A prognostic cloud fraction and condensation scheme. Part I: Scheme description. *Q. J. R. Meteorol. Soc.* **134**: 2093–2107.

Wilson DR, Bushell AC, Kerr-Munslow AM, Price D, Morcrette C, Bodas-Salcedo A. 2008b. PC2: A prognostic cloud fraction and condensation scheme. Part II: Results of climate model simulations. *Q. J. R. Meteorol. Soc.* **134**: 2109–2125.

Wu T, Yu R, Zhang F, Wang Z, Dong M, Wang L, Jin X, Chen D, Li L. 2010. The Beijing Climate Center atmospheric general circulation model: Description and its performance for the present-day climate. *Clim. Dyn.* **34**: 123–147, doi: 10.1007/s00382-008-0487-2.

Xie P, Arkin PA. 1997. Global precipitation: A 17-year monthly analysis based on gauge observations, satellite measurements and numerical model outputs. *Bull. Am. Meteorol. Soc.* **78**: 2539–2558.

Xin XG, Wu TW, Li JL, Wang ZZ, Li WP, Wu FH. 2013. How well dows the BCC-CSM1.1 reproduce the 20th century climate change over China? *Atmos. Oceanic Sci. Lett.* **6**: 21–26.

Yang GY, Slingo J. 2001. The diurnal cycle in the tropics. *Mon. Weather Rev.* **129**: 784–801.

Yukimoto S, Adachi Y, Hosaka M, Sakami T, Yoshimura H, Hirabara M, Tanaka TY, Shindo E, Tsujino H, Deushi M, Mizuta R, Yabu S, Obata A, Nakano H, Koshiro T, Ose T, Kitoh A. 2012. A new global climate model of the Meteorological Research Institute: MRI-CGCM3–model description and basic performance. *J. Meteorol. Soc. Jpn.* **90A**: 23–64.

